Research Article | Vol. 26, No. 12 | 11 Jun 2018 | OPTICS EXPRESS 15167

Optics EXPRESS

Frequency noise suppression of optical injection-locked quantum cascade lasers

XING-GUANG WANG,[1] BIN-BIN ZHAO,[1] FRÉDÉRIC GRILLOT,[2,3] AND CHENG WANG[1,*]

[1]School of Information Science and Technology, Shanghai Tech University, Shanghai 201210, China
[2]LTCI, Télécom ParisTech, Université Paris Saclay, 46 rue Barrault, F-75634 Paris Cedex 13, France
[3]Center for High Technology Materials, University of New Mexico, 1313 Goddard SE, Albuquerque, New Mexico 87106-4343, USA
*wangcheng1@shanghaitech.edu.cn

Abstract: This work theoretically investigates the frequency noise (FN) characteristics of quantum cascade lasers subject to the optical injection through a set of coupled rate equations with Langevin noise sources. It is shown that the low-frequency FN is completely suppressed by the optical injection, and the suppression bandwidth increases with the increasing injection ratio. The optimal FN peak suppression ratio at an injection ratio of 10 dB reaches 2.9 dB. In addition, it is found that the optical injection at positive frequency detunings close to the locking boundary invokes an additional peak in the FN spectrum, which can be higher than the carrier noise-induced one of free-running lasers. This peak amplitude strongly depends on the value of the linewidth broadening factor. Unlike injection-locked interband lasers, the FN peak does not necessarily exhibit a resonance.

OCIS codes: (140.5965) Semiconductor lasers, quantum cascade; (140.3520) Lasers, injection-locked; (270.2500) Fluctuations, relaxations, and noise; (290.3700) Linewidth.

References and links

1. J. Ohtsubo, *Semiconductor Lasers: Stability, Instability, and Chaos* (Springer, 2007).
2. S. Wieczorek, B. Krauskopf, T. B. Simpson, and D. Lenstra, "The dynamical complexity of optically injected semiconductor lasers," Phys. Rep. **416**(1–2), 1–128 (2005).
3. S. Saito, O. Nilsson, and Y. Yamamoto, "Frequency modulation noise and linewidth reduction in a semiconductor laser by means of a negative frequency feedback technique," Appl. Phys. Lett. **46**(1), 3–5 (1985).
4. C. Wang, F. Grillot, V. I. Kovanis, J. D. Bodyfelt, and J. Even, "Modulation properties of optically injection-locked quantum cascade lasers," Opt. Lett. **38**(11), 1975–1977 (2013).
5. T. Erneux, V. Kovanis, and A. Gavrielides, "Nonlinear dynamics of an injected quantum cascade laser," Phys. Rev. E **88**(3), 032907 (2013).
6. B. Meng and Q. J. Wang, "Theoretical investigation of injection-locked high modulation bandwidth quantum cascade lasers," Opt. Express **20**(2), 1450–1464 (2012).
7. H. Simos, A. Bogris, D. Syvridis, and W. Elsäßer, "Intensity noise properties of mid-infrared injection locked quantum cascade lasers: I. Modeling," IEEE J. Quantum Electron. **50**(2), 98–105 (2014).
8. M. S. Taubman, T. L. Myers, B. D. Cannon, and R. M. Williams, "Stabilization, injection and control of quantum cascade lasers, and their application to chemical sensing in the infrared," Spectrochim. Acta A Mol. Biomol. Spectrosc. **60**(14), 3457–3468 (2004).
9. C. Juretzka, H. Simos, A. Bogris, D. Syvridis, W. Elsäßer, and M. Carras, "Intensity noise properties of midinfrared injection locked quantum cascade lasers: II. Experiments," IEEE J. Quantum Electron. **51**(1), 2300208 (2015).
10. F. Bielsa, A. Douillet, T. Valenzuela, J. P. Karr, and L. Hilico, "Narrow-line phase-locked quantum cascade laser in the 9.2 μm range," Opt. Lett. **32**(12), 1641–1643 (2007).
11. S. Borri, I. Galli, F. Cappelli, A. Bismuto, S. Bartalini, P. Cancio, G. Giusfredi, D. Mazzotti, J. Faist, and P. De Natale, "Direct link of a mid-infrared QCL to a frequency comb by optical injection," Opt. Lett. **37**(6), 1011–1013 (2012).
12. B. Argence, B. Chanteau, O. Lopez, D. Nicolodi, M. Abgrall, C. Chardonnet, C. Daussy, B. Darquié, Y. Le Coq, and A. Amy-Klein, "Quantum cascade laser frequency stabilization at the sub-Hz level," Nat. Photonics **9**(7), 456–460 (2015).
13. J. R. Freeman, L. Ponnampalam, H. Shams, R. A. Mohandas, C. C. Renaud, P. Dean, L. Li, A. G. Davies, A. J. Seeds, and E. H. Linfield, "Injection locking of a terahertz quantum cascade laser to a telecommunications wavelength frequency comb," Optica **4**(9), 1059–1064 (2017).

#326537 https://doi.org/10.1364/OE.26.015167
Journal © 2018 Received 20 Mar 2018; revised 7 May 2018; accepted 17 May 2018; published 31 May 2018

Optics EXPRESS

14. X. G. Wang, F. Grillot, and C. Wang, "Rate equation modeling of the frequency noise and the intrinsic spectral linewidth in quantum cascade lasers," Opt. Express **26**(3), 2325–2334 (2018).
15. J. Faist, *Quantum Cascade Lasers* (Oxford, 2013).
16. R. Lang, "Injection locking properties of a semiconductor laser," IEEE J. Quantum Electron. **18**(6), 976–983 (1982).
17. C. Wang, F. Grillot, V. Kovanis, and J. Even, "Rate equation analysis of injection-locked quantum cascade lasers," J. Appl. Phys. **113**(6), 063104 (2013).
18. A. Murakami, K. Kawashima, and K. Atsuki, "Cavity resonance shift and bandwidth enhancement in semiconductor lasers with strong light injection," IEEE J. Quantum Electron. **39**(10), 1196–1204 (2003).
19. L. A. Coldren, S. W. Corzine, and M. L. Mašanović, Appendix 13 in *Diode Lasers and Photonic Integrated Circuits* (Wiley, 2012).
20. C. Harder, J. Katz, S. Margalit, J. Shacham, and A. Yariv, "Noise equivalent circuit of a semiconductor laser diode," IEEE J. Quantum Electron. **18**(3), 333–337 (1982).
21. S. Borri, S. Bartalini, P. C. Pastor, I. Galli, G. Giusfredi, D. Mazzotti, M. Yamanishi, and P. De Natale, "Natale, "Frequency-noise dynamics of mid-infrared quantum cascade lasers," IEEE J. Quantum Electron. **47**(7), 984–988 (2011).
22. M. Yamanishi, "Theory of intrinsic linewidth based on fluctuation-dissipation balance for thermal photons in THz quantum-cascade lasers," Opt. Express **20**(27), 28465–28478 (2012).
23. Y. Petitjean, F. Destic, J. C. Mollier, and C. Sirtori, "Dynamic modeling of Terahertz quantum cascade lasers," IEEE J. Sel. Top. Quantum Electron. **17**(1), 22–29 (2011).
24. F. Rana and R. J. Ram, "Current noise and photon noise in quantum cascade lasers," Phys. Rev. B **65**(12), 125313 (2002).
25. M. K. Haldar, "A simplified analysis of direct intensity modulation of quantum cascade laser," IEEE J. Quantum Electron. **41**(11), 1349–1355 (2005).
26. J. Faist, L. Ajili, G. Scalari, M. Giovannini, M. Beck, M. Rochat, H. Beere, A. G. Davies, E. H. Linfield, and D. Ritchie, "Terahertz quantum cascade lasers," Philos Trans A Math Phys Eng Sci **362**(1815), 215–231 (2004).
27. C. Sirtori, "GaAs Quantum cascade laser: fundamentals and performances," EDP sciences **7**(3), 1– 20 (2002).
28. J. von Staden, T. Gensty, W. Elsässer, G. Giuliani, and C. Mann, "Measurements of the α factor of a distributed-feedback quantum cascade laser by an optical feedback self-mixing technique," Opt. Lett. **31**(17), 2574–2576 (2006).
29. T. Aellen, R. Maulini, R. Terazzi, N. Hoyler, M. Giovannini, J. Faist, S. Blaser, and L. Hvozdara, "Direct measurement of the linewidth enhancement factor by optical heterodyning of an amplitude-modulated quantum cascade laser," Appl. Phys. Lett. **89**(9), 091121 (2006).
30. T. Liu, K. E. Lee, and Q. J. Wang, "Importance of the microscopic effects on the linewidth enhancement factor of quantum cascade lasers," Opt. Express **21**(23), 27804–27815 (2013).
31. M. F. Pereira, "The linewidth enhancement factor of intersubband lasers: From a two-level limit to gain without inversion conditions," Appl. Phys. Lett. **109**(22), 222102 (2016).
32. C. Henry, "Theory of the linewidth of semiconductor lasers," IEEE J. Quantum Electron. **18**(2), 259–264 (1982).
33. C. Wang, K. Schires, M. Osiński, P. J. Poole, and F. Grillot, "Thermally insensitive determination of the linewidth broadening factor in nanostructured semiconductor lasers using optical injection locking," Sci. Rep. **6**(1), 27825 (2016).
34. P. Gallion, H. Nakajima, G. Debarge, and C. Chabran, "Contribution of spontaneous emission to the linewidth of an injection-locked semiconductor laser," Electron. Lett. **21**(14), 626–628 (1985).
35. S. Saito, F. Mogensen, and H. Olesen, "Effective bandwidth for FM noise suppression in an injection-locked semiconductor laser," Electron. Lett. **21**(24), 1173–1175 (1985).
36. F. Mogensen, H. Olesen, and G. Jacobsen, "FM noise suppression and linewidth reduction in an injection-locked semiconductor laser," Electron. Lett. **21**(16), 696–697 (1985).
37. T. B. Simpson, J. M. Liu, and A. Gavrielides, "Bandwidth enhancement and broadband noise reduction in injection-locked semiconductor lasers," IEEE Photonics Technol. Lett. **7**(7), 709–711 (1995).
38. G. Yabre, H. de Waardt, H. P. A. Van den Boom, and G.-D. Khoe, "Noise characteristics of single-mode semiconductor lasers under external light injection," IEEE J. Quantum Electron. **36**(3), 385–393 (2000).
39. E. K. Lau, L. J. Wong, and M. C. Wu, "Enhanced Modulation Characteristics of Optical Injection-Locked Lasers: A Tutorial," IEEE J. Sel. Top. Quantum Electron. **15**(3), 618–633 (2009).
40. D. J. Higham, "An algorithmic introduction to numerical simulation of stochastic differential equations," SIAM Rev. **43**(3), 525–546 (2001).
41. G. Di Domenico, S. Schilt, and P. Thomann, "Simple approach to the relation between laser frequency noise and laser line shape," Appl. Opt. **49**(25), 4801–4807 (2010).

1. Introduction

The optical injection technique synchronizes one laser of high spectral purity (master laser) with another laser (slave laser) through an optical isolator. Semiconductor lasers subject to the optical injection produces a large variety of nonlinear dynamics including stable injection locking, periodic and aperiodic pulsations, and chaotic oscillations [1]. The stable locking

Optics EXPRESS

regime is bounded by the Hopf bifurcation and the saddle-node bifurcation, where the phase of the slave laser is synchronized to that of the master laser [2]. Inside the injection locking regime, the optical injection can considerably improve dynamical performances of semiconductor lasers, including enhancement of the modulation bandwidth, reduction of the frequency chirp, as well as suppression of the relative intensity noise (RIN) and the frequency noise (FN, or phase noise) [3]. Owing to the above benefits, the injection locking technique attracts increasing interests for quantum cascade lasers (QCLs) as well. In recent years, researchers have theoretically investigated the injection locking regime [4,5], the modulation bandwidth enhancement properties [6], and the RIN suppression characteristics [7] of QCLs subject to the optical injection. In experiments, Taubman *et al.* demonstrated a locking range of 1.0 GHz at an injection ratio of −16 dB [8]. Juretzka *et al.* proved that the RIN of a QCL was reduced up to 10 dB by the optical injection [9]. On the other hand, most work employs the optical injection to narrow the spectral linewidth of QCLs. Bielsa *et al.* locked a 9.2 μm QCL to a single-mode CO_2 laser, and reduced the laser linewidth from several MHz down to the kilohertz range [10]. An alternative popular method is locking mid-infrared or terahertz QCLs to near-infrared optical frequency combs through the difference-frequency generation process, where the linewidth of QCLs is governed by the frequency comb [11–13].

In our recent work, it was demonstrated theoretically that the FN spectrum of free-running QCLs exhibited a broad peak due to the carrier noise induced carrier variation [14]. In this work, we theoretically investigate the FN characteristics of a QCL subject to the optical injection. It is found that the optical injection significantly suppresses the FN of QCLs in the low frequency range, and the suppression bandwidth increases with the injection strength. At an injection ratio of 10 dB, the optimal FN peak suppression ratio reaches 2.9 dB, which is achieved at detuning frequency of −3.3 GHz. In addition, the optical injection at frequency detuning close to the positive locking boundary invokes a peak in the FN spectrum, and the peak amplitude is strongly dependent on the linewidth broadening factor.

2. Rate equation model of injection-locked QCLs

The electronic structure model of the QCL takes into account the upper laser level, the lower laser level, and the bottom level [4]. Electrons are firstly injected from the injector region into the upper laser level in the gain region. Then, electrons scatter into the lower laser level with a time τ_{32}, and into the bottom level with a time τ_{31} through longitudinal-optical phonon emissions [15]. Subsequently, electrons in the lower laser level deplete into the bottom level with a time τ_{21}, and finally escape the gain region with a tunneling out time τ_{out} into the next stage. The stimulated emission occurs upon the population inversion between the upper and the lower laser levels. Correspondingly, the rate equations describing the carrier numbers in the upper level (N_3), in the lower level (N_2), and in the bottom level (N_1) are given by

$$\frac{dN_3}{dt} = \eta\frac{I}{q} - \frac{N_3}{\tau_{32}} - \frac{N_3}{\tau_{31}} - G_0\Delta NS + F_3(t) \tag{1}$$

$$\frac{dN_2}{dt} = \frac{N_3}{\tau_{32}} - \frac{N_2}{\tau_{21}} + G_0\Delta NS + F_2(t) \tag{2}$$

$$\frac{dN_1}{dt} = \frac{N_3}{\tau_{31}} + \frac{N_2}{\tau_{21}} - \frac{N_1}{\tau_{out}} + F_1(t) \tag{3}$$

where I is the pump current, η is the current injection efficiency, G_0 is the gain coefficient, and ΔN is the population inversion as $\Delta N = N_3$-N_2. Based on the classical injection-locking model developed by [16], the photon number (S) and the phase (ϕ) of the injection-locked QCL are derived as

Optics EXPRESS

$$\frac{dS}{dt}=\left(mG_0\Delta N-\frac{1}{\tau_p}\right)S+m\beta\frac{N_3}{\tau_{sp}}+2k_c\sqrt{S_{inj}S}\cos\phi+F_S(t) \tag{4}$$

$$\frac{d\phi}{dt}=\frac{\alpha_H}{2}\left(mG_0\Delta N-\frac{1}{\tau_p}\right)-2\pi\Delta F_{inj}-k_c\sqrt{\frac{S_{inj}}{S}}\sin\phi+F_\phi(t) \tag{5}$$

where τ_p is the photon lifetime, τ_{sp} is the spontaneous emission lifetime, β is the spontaneous emission factor, α_H is the linewidth broadening factor (LBF), and m is the gain stage number. S_{inj} is the photon number of the master laser, and the injection ratio is defined as $R_{inj} = S_{inj}/S_0$, with S_0 being the photon number of the free-running laser. ΔF_{inj} is the frequency detuning defined as the lasing frequency difference between the master laser and the slave laser. k_c is the coupling coefficient of the two lasers as $k_c = v_g(1-R)/(2L\sqrt{R})$, with v_g being the light group velocity, L being the laser cavity length, and R being the facet reflectivity [17,18].

The rate equation model includes the carrier noise and the spontaneous emission noise through the Langevin approach [19]. The time averages of all the carrier ($F_{3,2,1}$), photon (F_S), and phase (F_ϕ) noise sources are zero due to the random nature [20], and the correlation relations of the noise sources are:

$$\left\langle F_i(t)F_j(t')\right\rangle=U_{ij}\delta(t-t') \tag{6}$$

with the correlation strengths

$$\begin{aligned}
&U_{33}=2(G_0N_3S+N_3/\tau_{32}+N_3/\tau_{31});\ U_{22}=2(G_0N_3S+N_3/\tau_{32})\\
&U_{SS}=2m(G_0N_3S+\beta N_3/\tau_{sp});\ U_{\phi\phi}=2m(G_0N_3S+\beta N_3/\tau_{sp})/(4S^2)\\
&U_{32}=-(G_0N_3S+G_0N_2S+N_3/\tau_{32});\ U_{3S}=-(G_0N_3S+G_0N_2S+\beta N_3/\tau_{sp})\\
&U_{2S}=(G_0N_3S+G_0N_2S+\beta N_3/\tau_{sp});\ U_{3\phi}=U_{2\phi}=U_{S\phi}=0
\end{aligned} \tag{7}$$

where correlations related to F_1 are not listed, because F_1 does not contribute to the FN of QCLs. It is remarked that the noise of the master laser is not considered in the above rate equation model. In addition, technical noise (flicker noise) and thermal photon noise of the QCL are not included as well [21,22]. In the following sections, the steady-state solutions and the optical spectra are calculated through the numerical approach, while the FN spectra are obtained through the semi-analytical approach.

Table 1. QCL material and optical parameters [23–27]

Symbol	Description	Value
G_0	Gain coefficient	5.3×10^4 /s
τ_p	Photon lifetime	3.7 ps
τ_{sp}	Spontaneous emission time	7.0 ns
β	Spontaneous emission factor	1.0×10^{-6}
α_H	Linewidth broadening factor	0.5
m	Gain stage number	30
τ_{32}	Scattering time upper to lower	2.0 ps
τ_{31}	Scattering time upper to bottom	2.4 ps
τ_{21}	Scattering time lower to bottom	0.5 ps
τ_{out}	Tunneling out time	0.5 ps
k_c	Injection coupling coefficient	2.0×10^{10} /s

3. Results and discussion

Table 1 lists the QCL parameters used for the simulations in this work, unless stated otherwise [23–27]. The free-running QCL exhibits a lasing threshold current of I_{th} = 223 mA,

Optics EXPRESS

and the laser is pumped at $1.5 \times I_{th}$ in all the simulations of this work. Based on the analysis of the integrated time series of the photon number, Fig. 1 illustrates the stable injection-locking boundaries, which are formed by the Hopf bifurcation and the saddle-node bifurcation [2,4]. The same as interband semiconductor lasers, the two bifurcations strongly depend on the value of LBF. QCLs usually show near-zero LBFs, and the reported values range from 0 up to 3.0 [28, 29]. The non-zero LBF in QCLs has been found to originate from the non-parabolicity of the band structure, the many-body effect, the resonant tunneling transport, as well as the counter-rotating wave contribution [30, 31]. The bifurcation diagram is symmetric for a zero LBF, while a non-zero LBF leads to an asymmetric diagram. The stable locking regime broadens with the increasing LBF—at an injection ratio of 0 dB, the locking range increases from 6.4 GHz for $\alpha_H = 0$ to 15.3 GHz for $\alpha_H = 2.0$. In the following sections, we discuss the injection strength effect and the frequency detuning effect on the FN spectrum of QCLs within the stable locking regime, respectively.

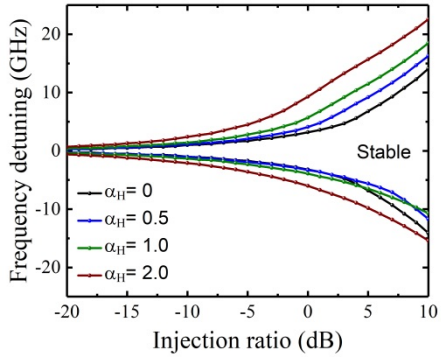

Fig. 1. Stable locking boundaries of the QCL for different LBFs.

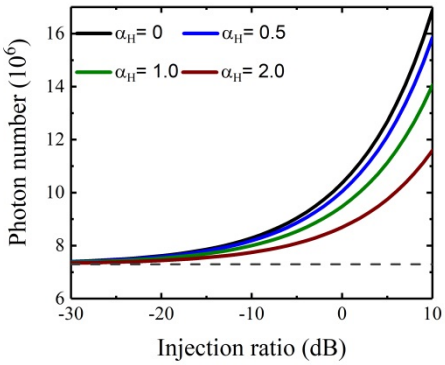

Fig. 2. Injection strength effect on the photon number at zero detuning. The dashed line indicates that of the free-running laser.

3.1 Injection strength effect on the FN

Within the stable locking regime, the steady-state solutions of the injection-locked QCL are derived as

Optics EXPRESS

$$S = \frac{k_c^2 R_{inj} S_0}{\frac{1}{4}\left(\frac{1}{\tau_p} - mG_0\Delta N\right)^2 + \left[\frac{\alpha_H}{2}\left(mG_0\Delta N - \frac{1}{\tau_p}\right) - 2\pi\Delta F_{inj}\right]^2} \tag{8}$$

$$\Delta N = \frac{1}{mG_0}\left(\frac{1}{\tau_p} - 2k_c\sqrt{\frac{R_{inj}S_0}{S}}\cos\phi\right) \tag{9}$$

$$\phi = \sin^{-1}\left(\frac{-2\pi\Delta F_{inj}}{k_c\sqrt{1+\alpha_H^2}}\sqrt{\frac{S}{R_{inj}S_0}}\right) - \tan^{-1}\alpha_H \tag{10}$$

It will be shown that the above formulas are helpful for understanding the injection strength and the frequency detuning effects on the FN characteristics. Figure 2 shows the injection strength effect on the photon number at zero frequency detuning. As suggested in Eq. (8), the photon of the injection-locked QCL at zero detuning increases with the injection ratio while decreases with the LBF [17].

In rating Eqs. (1)-(5), all the noise sources perturb the laser system slightly away from the steady-state condition. Based on the standard small-signal analysis in the Appendix, the FN spectrum of the injection-locked QCL is calculated by [19]:

$$FN(f) = f^2\left|\delta\varphi(f)\right|^2 \tag{11}$$

with $\delta\varphi$ being the phase variation due to the noise perturbation. When the Fourier frequency approaches zero or infinite, the FN of the injection-locked QCL becomes

$$FN(f \to 0) = 0 \tag{12}$$

$$FN(f \to \infty) = \frac{m\left(G_0 N_3 S + \beta N_3/\tau_{sp}\right)}{8\pi^2 S^2} \approx \frac{mG_0 N_3}{8\pi^2 S} \tag{13}$$

For $f \to 0$, the FN of the QCL is reduced to zero because the master laser has no optical noise. For $f \to \infty$, the FN is linearly proportional to the carrier population N_3 in the upper laser level, while inversely proportional to the photon number S.

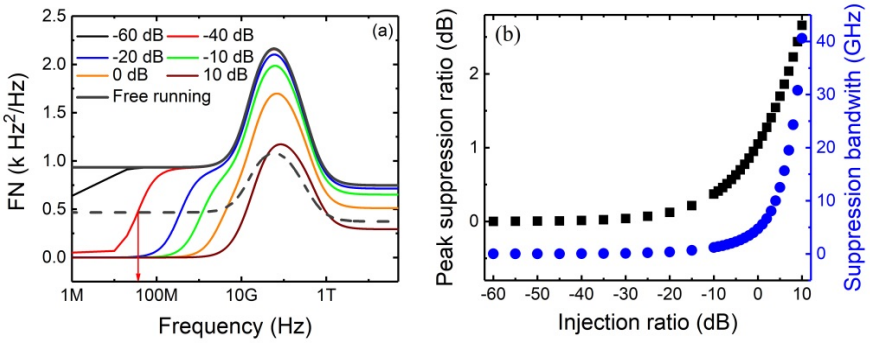

Fig. 3. (a) Injection strength effect on the FN at zero detuning for $\alpha_H = 0.5$. The dashed curve is –3 dB of the free-running laser's FN, and the arrow indicates the suppression bandwidth. (b) The suppression ratio of the FN peak (squares) and the suppression bandwidth (circles) as a function of the injection ratio.

Optics EXPRESS

Figure 3(a) shows that the FN of the free-running QCL is almost constant at 930 Hz^2/Hz for low frequencies up to 1.0 GHz. Interestingly, the FN exhibits a broad peak in the frequency range of 10 GHz to 1.0 THz, which is due to the carrier noise perturbation based on our previous analysis [14]. Beyond 10 THz, the FN becomes almost flat at 746 Hz^2/Hz, which is determined solely by the spontaneous emission noise. The difference between the low- and high-frequency FN is governed by a factor of $(1+\alpha_H^2)$ [32]. When the QCL is subject to the optical injection, the FN in the whole frequency range is reduced, partly owing to the increase of the photon number, the decrease of the carrier number in the upper laser level, as well as the reduction of the threshold gain [33]. The low-frequency FN undergoes the largest reduction, down to almost zero as expressed in Eq. (12). This is because the low-frequency phase of the slave laser is strongly locked to that of the master laser without any noise. In case the rate equations take into account the optical noise of the master laser, which has no correlation with that of the slave laser, the low-frequency FN will be the same as that of the master laser [34–36]. Therefore, like injection-locked interband lasers, the spectral linewidth of the injection-locked QCL is only governed by the FN of the master laser, and no longer follows the Schawlow-Townes limit of the free-running laser [34]. It is worthwhile to mention that the relative intensity noise of injection-locked interband lasers is dominated by the master laser as well, and the injection-locked QCL is expected to exhibit a similar behavior [37,38].

In order to quantitatively characterize this low frequency range, we simply define the suppression bandwidth, within which the FN is lower than −3 dB of the FN in the free-running QCL (arrow in Fig. 3(a)). Thus, the FN below the suppression bandwidth is primarily determined by the master laser, while that above the bandwidth is mainly governed by the slave laser. Figure 3(b) presents that the FN suppression bandwidth (circles) increases with the injection strength from 4.0 MHz at R_{inj} = –60 dB up to 40 GHz at R_{inj} = 10 dB. However, a more rigorous definition of the FN suppression bandwidth for QCLs is required in future work. For interband lasers, the FN suppression bandwidth is found to be half-width of the stable locking bandwidth at α_H = 0 [34, 35]. In order to characterize the FN suppression effect, the suppression ratio of the FN peak is defined as the peak amplitude of the free-running laser divided by that of the injection-locked laser. Obviously, the FN peak suppression ratio (squares) in Fig. 3(b) increases with the injection strength and reaches 2.7 dB at R_{inj} = 10 dB.

3.2 Frequency detuning effect on the FN

Figure 4 shows the frequency detuning effect on the photon number of the QCL at an injection ratio of 0 dB. For α_H = 0, the maximum photon number occurs at zero frequency detuning, and the curve is symmetric for both negative and positive detunings as indicated in Eq. (8). On the other hand, the maximum photon number for non-zero LBFs is achieved at a negative detuning, where the phase difference ϕ between the master laser and the slave laser is found to be zero. For any LBF, the photon number of the injection-locked laser converges to the free running one (dashed line) at the detuning of $\Delta F_{inj} = k_c\sqrt{R_{inj}}/2\pi$ (3.2 GHz), where the population inversion meets $mG_0\Delta N = 1/\tau_p$ in Eq. (8).

Figure 5 shows the frequency detuning effect on the FN at R_{inj} = 0 dB for different values of LBF. For α_H = 0 in Fig. 5(a), the FN of the free-running laser (dashed line) is constant over the whole frequency range. The minimum FN is achieved at zero frequency detuning while both the negative and the positive detunings raise the FN symmetrically. In addition, both frequency detunings lead to the appearance of a peak in the FN spectrum, and the peak amplitude becomes higher than the free-running case when the detuning is operated close to the locking boundaries (± 3.2 GHz). For non-zero LBFs in Figs. 5(b) and 5(c), the minimum FN is also achieved at a phase difference of zero, where the photon number S reaches

Optics EXPRESS

maximum (see Fig. 4) and the carrier number in the upper laser level N_3 reaches minimum (see Eq. (13)) . In addition, the FN peak increases with increasing frequency detuning. At some positive detunings (4.0 GHz in Fig. 5(b) and 5.0, 7.0, 9.0 GHz in Fig. 5(c)), the optical injection invokes another peak in the FN spectrum in addition to the carrier noise induced one of the free-running laser. The frequency of the peak arising from the optical injection is smaller, while the amplitude of the peak is higher than the latter one. Especially for $\alpha_H = 2.0$ in Fig. 5(c), the FN near the positive locking boundary (9.0 GHz) exhibits a giant peak, which is five times higher than the free-running case. The appearance of the giant peak near the positive locking boundary is similar to that of injection-locked interband lasers [18,39]. The peak in interband lasers is attributed to the underdamped resonance arising from the transient interference between the injection-locked field and the shifted cavity-resonance field [18]. However, it is found that the injection-locked QCL only exhibits a resonance for detunings at 0, 5.0, 7.0, and 9.0 GHz in Fig. 5(c), while the other cases in Fig. 5 do not have any resonance. Thus, the physical mechanism for the peak appearance in QCLs is different to that in interband lasers, which requires further investigation in future work. In addition, the FN peak frequency decreases with increasing detuning frequency at the positive detuning side, which is opposite in interband lasers. The peak frequency eventually merges with the Hopf frequency at the positive locking boundary.

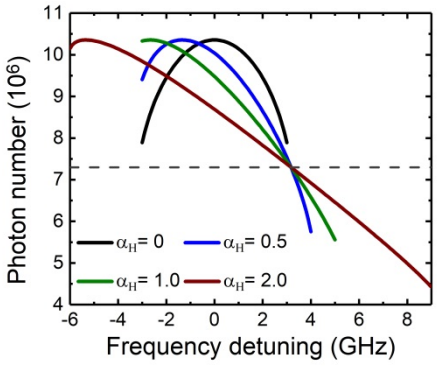

Fig. 4. Frequency detuning effect on the photon number at R_{inj} = 0 dB. The dashed line indicates that of the free-running laser.

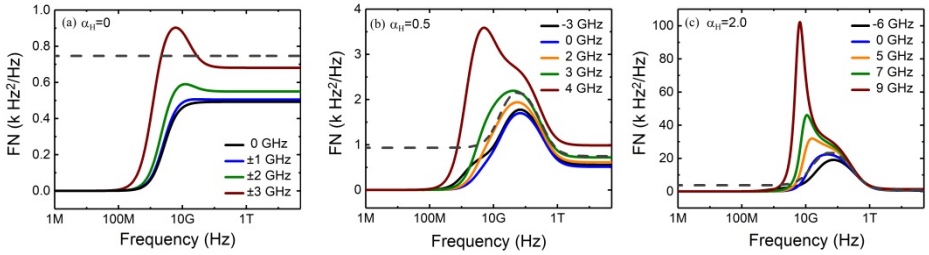

Fig. 5. Frequency detuning effect on the FN for (a) α_H = 0, (b) α_H = 0.5, and for (c) α_H = 2.0 at R_{inj} = 0 dB. The dashed curves indicate that of the free-running laser.

Figure 6(a) illustrates the suppression ratio diagram of the FN peak formed by the injection ratio and the detuning frequency at α_H = 0.5. It is shown that the FN peak of the injection-locked QCL is mostly lower than that of the free-running laser, except at very positive detuning frequencies. The detuning frequency for achieving the maximum suppression ratio (dashed line) reduces with the injection ratio, from −1.4 GHz at R_{inj} = 0 dB down to −3.3 GHz at R_{inj} = 10 dB. Figure 6(b) shows that the detuning frequency for

Optics EXPRESS

obtaining the maximum suppression bandwidth (dashed line) also decreases with the injection ratio, from –0.9 GHz at R_{inj} = 0 dB down to –3.3 GHz at R_{inj} = 10 dB.

Figure 7 simulates the optical spectra of the injection-locked QCL at R_{inj} = 0 dB, through integrating rate Eqs. (1)-(5) using the Euler-Maruyama method [40]. The time integration step is 0.1 ps, the integration length is 1.0 μs, and each integration costs about nine-hour computational time. The spectral linewidth of the injection-locked QCL is almost zero for any LBF, because the linewidth is determined only by the low-frequency (<100 MHz) FN, which is zero in Fig. 5 [41]. For α_H = 2.0, the optical spectrum of the injection-locked QCL exhibits two side peaks (arrows), which arise from the giant FN peak in Fig. 5(c). The frequency separation between the side peaks and the central lasing peak is about 6.0 GHz, corresponding to the FN peak frequency.

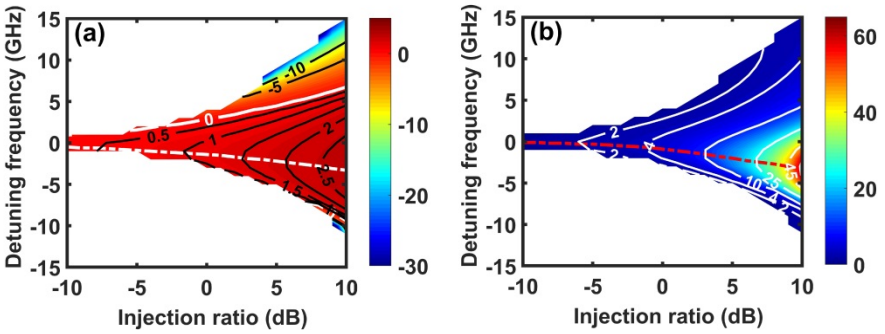

Fig. 6. (a) FN peak suppression ratio (in dB), the dashed line indicates the maximum suppression ratio, and the thick-white curve highlights the 0-dB suppression ratio. (b) FN suppression bandwidth (in GHz), the dashed line indicates the maximum suppression bandwidth. The LBF is set at α_H = 0.5.

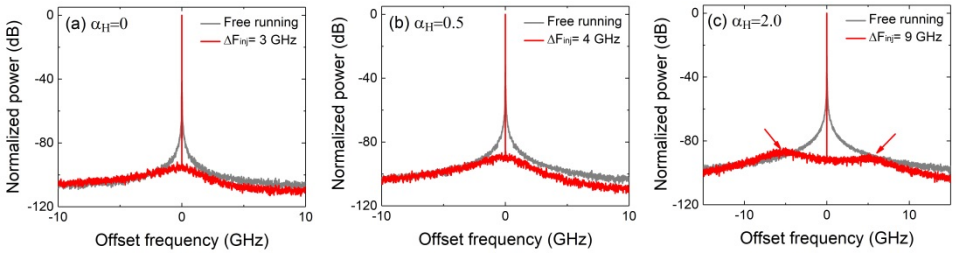

Fig. 7. Simulated optical spectra of the injection-locked QCL at R_{inj} = 0 dB for (a) α_H = 0, (b) α_H = 0.5, and (b) α_H = 2.0. The optical power is normalized to that of the spectral peak. The arrows indicate the side peaks.

4. Conclusions

In conclusion, the injection strength and the frequency detuning effects on the FN characteristics of the QCL have been numerically investigated through the rate equations. It is shown that the stable locking regime is broadened by a large LBF. The FN decreases with the increasing injection ratio, and the low-frequency FN reduces to zero when the master laser has no optical noise. The optical injection at positive detuning close to the locking boundary induces a peak in the FN spectrum, and the peak amplitude strongly depends on the LBF. In contrast to interband lasers, the injection-induced FN peak in QCLs does not necessarily have a resonance. In addition, the giant FN peak leads to the appearance of side peaks in the optical spectrum of the injection-locked QCL. Future work will take into account the optical noise of the master laser, and will investigate the optical feedback effect on the FN of QCLs.

Optics EXPRESS

Appendix,: Small-signal analysis of the rate equations

In the small-signal analysis of rate Eqs. (1)-(5), all the Langevin noise sources drive the laser system away from its steady-state solutions. The small-signal responses of the carriers, the photon, and the phase are written as

$$\begin{aligned} &\mathrm{N}_3(t) = N_3^0 + \delta n_3(\omega)e^{j\omega t};\ \mathrm{N}_2(t) = N_2^0 + \delta n_2(\omega)e^{j\omega t},\ \mathrm{N}_1(t) = N_1^0 + \delta n_1(\omega)e^{j\omega t}, \\ &S(t) = S^0 + \delta s(\omega)e^{j\omega t},\ \phi(\mathrm{t}) = \phi^0 + \delta\varphi(\omega)e^{j\omega t}. \end{aligned} \tag{14}$$

where $N_{3,2,1}^0$, S^0, and ϕ^0 are the steady-state solutions, and ω is the angular frequency. Substituting Eq. (14) into rate Eqs. (1)-(5), and neglecting harmonic frequency terms, we obtain the linearized differential rate equations in the form of matrix as

$$\begin{bmatrix} j\omega+\gamma_{11} & -\gamma_{12} & 0 & \gamma_{14} & 0 \\ -\gamma_{21} & j\omega+\gamma_{22} & 0 & -\gamma_{24} & 0 \\ -\gamma_{31} & -\gamma_{32} & j\omega & 0 & 0 \\ -\gamma_{41} & \gamma_{42} & 0 & j\omega+\gamma_{44} & \gamma_{45} \\ -\gamma_{51} & \gamma_{52} & 0 & -\gamma_{54} & j\omega+\gamma_{55} \end{bmatrix} \begin{bmatrix} \delta n_3(\omega) \\ \delta n_2(\omega) \\ \delta n_1(\omega) \\ \delta s(\omega) \\ \delta\phi(\omega) \end{bmatrix} = \begin{bmatrix} F_3 \\ F_2 \\ F_1 \\ F_s \\ F_\phi \end{bmatrix} \tag{15}$$

with the parameters

$$\begin{aligned} &\gamma_{11} = \tau_{32}^{-1} + \tau_{31}^{-1} + G_0 S^0,\ \gamma_{12} = G_0 S^0,\ \gamma_{14} = G_0 \Delta N^0, \\ &\gamma_{21} = \tau_{32}^{-1} + G_0 S^0,\ \gamma_{22} = \tau_{21}^{-1} + G_0 S^0,\ \gamma_{24} = G_0 \Delta N^0, \\ &\gamma_{31} = \tau_{31}^{-1},\ \gamma_{32} = \tau_{21}^{-1},\ \gamma_{41} = m\left(\beta\tau_{sp}^{-1} + G_0 S^0\right),\ \gamma_{42} = mG_0 S^0, \\ &\gamma_{44} = \tau_p^{-1} - mG_0\Delta N^0 - k_c\sqrt{S_{inj}/S^0}\cos\phi^0,\ \gamma_{45} = 2k_c\sqrt{S_{inj} * S^0}\sin\phi^0, \\ &\gamma_{51} = \alpha_H mG_0/2,\ \gamma_{52} = \alpha_H mG_0/2,\ \gamma_{54} = k_c\sqrt{S_{inj}/S^0}\sin\phi/2S^0, \\ &\gamma_{55} = k_c\sqrt{S_{inj}/S^0}\cos\phi^0. \end{aligned} \tag{16}$$

Following Cramer's rule, we obtain the FN spectrum through Eq. (11) based on the semi-analytical approach.

Funding

Shanghai Pujiang Program (17PJ1406500).